

From InSb Nanowires to Nanocubes: Looking for the Sweet Spot

Sébastien R. Plissard,^{*,†} Dorris R. Slapak,[†] Marcel A. Verheijen,^{†,‡} Moïra Hocevar,[§] George W. G. Immink,[‡] Ilse van Weperen,[§] Stevan Nadj-Perge,[§] Sergey M. Frolov,[§] Leo P. Kouwenhoven,[§] and Erik P. A. M. Bakkers^{†,§}

[†]Department of Applied Physics, Eindhoven University of Technology, 5600 MB Eindhoven, The Netherlands

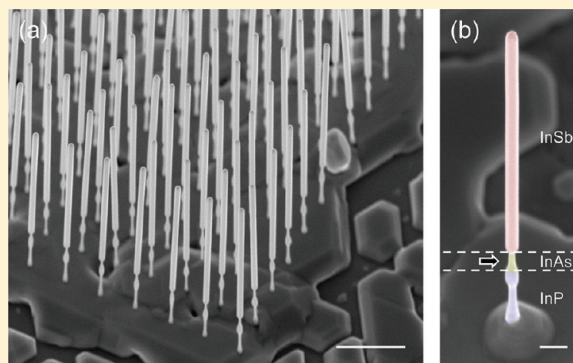
[‡]Philips Innovation Services, 5656 AE Eindhoven, The Netherlands

[§]Kavli Institute of Nanoscience, Delft University of Technology, 2600 GA Delft, The Netherlands

S Supporting Information

ABSTRACT: High aspect ratios are highly desired to fully exploit the one-dimensional properties of indium antimonide nanowires. Here we systematically investigate the growth mechanisms and find parameters leading to long and thin nanowires. Variation of the V/III ratio and the nanowire density are found to have the same influence on the “local” growth conditions and can control the InSb shape from thin nanowires to nanocubes. We propose that the V/III ratio controls the droplet composition and the radial growth rate and these parameters determine the nanowire shape. A sweet spot is found for nanowire interdistances around 500 nm leading to aspect ratios up to 35. High electron mobilities up to $3.5 \times 10^4 \text{ cm}^2 \text{ V}^{-1} \text{ s}^{-1}$ enable the realization of complex spintronic and topological devices.

KEYWORDS: Nanowire, nanocubes, InSb, growth mechanisms, arrays, mobility



Because of their homogeneous quasi one-dimensional shape, nanowires represent a system in which quantum dots can be defined with perfect control at the single photon and single electron level. Universal control of the spin–orbit state of a single electron has been demonstrated in pure wurtzite indium arsenide (InAs) nanowire quantum dots,¹ thanks to the strong spin–orbit interaction and large Landé g-factors of order 10. Recently, several groups reported the growth of InSb nanowires by metal–organic vapor phase epitaxy (MOVPE),² chemical beam epitaxy (CBE),^{3,4} and their integration in field effect transistors (FET).^{5–8} These nanowires are expected to exhibit even more advantageous properties for spin-based devices since high g-factors were reported,⁹ and because pure zinc-blende crystalline structure can be achieved for a large set of temperatures and V/III ratios.¹⁰ In addition, bulk InSb has a small bandgap (0.17 eV) and a high electron mobility ($77\,000 \text{ cm}^2/(\text{V s})$) in part due to the small electron mass ($0.015 m_e$). With these unique properties, InSb nanowires are expected to fulfill strict material requirements for the detection of Majorana fermions in tunable semiconductor/superconductor hybrid devices.^{11,12} There are, however, remaining challenges to meet on nanowire geometry and the electronic quality. The diameter should be below 100 nm for electrostatic gating and the length should be several micrometers for the establishment of a robust topological superconducting phase. In addition, the mean free path for electrons should be at least a few hundred nanometers. In this Letter, high aspect ratio and high electron mobility InSb nanowires are obtained. By analyzing the growth

mechanisms we find an aspect ratio “sweet spot” with optimized nanowire interdistance and V/III ratio.

Electron beam lithography is used to define ordered arrays of Au islands on (111)B InP substrates, and after gold deposition and lift-off the resulting droplets have a cylindrical shape with diameters ranging from 25 to 100 nm and a height of 6 nm. Arrays of 25×25 droplets with pitches ranging from 200 nm to $2 \mu\text{m}$ are fabricated. Prior to the loading into the MOVPE reactor a piranha etch is performed to remove resist residues. Before growth, the samples are annealed at $660 \text{ }^\circ\text{C}$ for 10 min under phosphine flow to form a gold indium (Au–In) alloy. This substrate preparation ensures well-controlled local reaction conditions and accurate statistics for determining the growth mechanisms. We use an InP–InAs stem for the growth of InSb. The InP is used to facilitate uniform nucleation, and the InAs is used to reduce the lattice mismatch with InSb. The substrate temperature is set to $420 \text{ }^\circ\text{C}$ during the InP and InAs stem growth leading to a mixed crystalline structure for InP and to a pure zinc-blende for InAs. The InSb nanowires are grown subsequently at $470 \text{ }^\circ\text{C}$ for 20 min using trimethylindium (TMI) and trimethylantimony (TMSb) with molar fractions of 7.6×10^{-6} and 3.4×10^{-4} , respectively (see details in Supporting Information, Section S1).

Received: November 1, 2011

Revised: February 7, 2012

The scanning electron microscopy (SEM) image in Figure 1a shows that uniform nanowire arrays can be obtained. Aspect

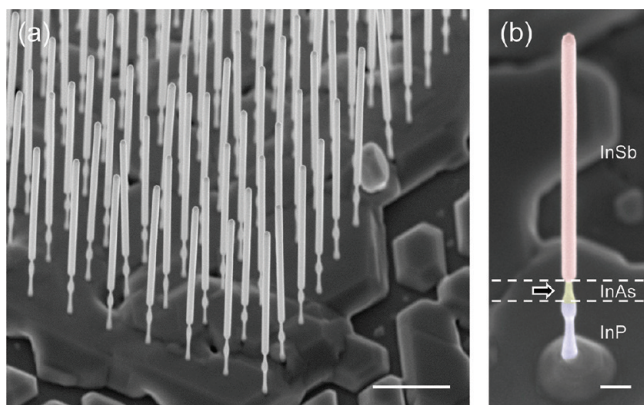


Figure 1. The 30° tilted SEM images of an InSb nanowire array. (a) Low-magnification image of a 25×25 nanowire array with a yield of over 95% grown using optimized parameters for 50 nm droplets: pitch = 500 nm and V/III = 26.4. Scale bar corresponds to 1 μm . (b) High-magnification image of a single nanowire. Color indicates the stacking of materials: InP (blue), InAs (yellow), and InSb (red). The arrow shows the zone in which the InAs stem evaporates. Scale bar corresponds to 200 nm.

ratios up to 35 (100 nm in diameter and 3.5 μm in length) are achieved under optimized growth conditions, which will be discussed below. From an image of a single nanowire (Figure 1b), it is clear that the InSb nanowire diameter is larger than that of the InAs segment. This diameter increase has been assigned to an increased particle volume due to the uptake of indium and to the rotation of the nanowire sidewalls.^{3,10} Notably, the InAs diameter decreases during the InSb nanowire growth, whereas the InP stem remains constant in diameter (see Supporting Information, section S7). We believe that at the high temperature (470 °C) used in this study arsenic

evaporates, thinning the InAs stem. For InSb growth times exceeding a critical time of 30 min, the InAs stem disappears and the nanowire breaks. The length of the InAs segment does not affect the evaporation rate, and for this system the thinning of the InAs is the limiting factor for the growth of longer InSb nanowires. Transmission electron microscopy (TEM) measurements on the morphology and interfaces of the heterostructure confirm the pure zinc-blende structure of both InAs and InSb segments and sharp interfaces between them (see Supporting Information, Section S2). Since the diameter increase is readily visible with SEM, this technique has been used in this study to further characterize the InSb nanowire growth.

The nanowire shape has been qualitatively investigated as a function of the V/III ratio, and the wire-to-wire distance. Figure 2a–d shows the morphology evolution of the InSb segment when increasing the V/III ratio from 44 to 166 (by keeping the TMI flow constant and increasing the TMSb flow) for a constant pitch of 500 nm and a droplet diameter of 50 nm. The yield exceeds 90%, enabling statistical analysis of lengths and diameters. In this series the InSb morphology evolves from thin and long nanowires (Figure 1a, aspect ratio ~ 14), to thick and short nanowires (Figure 1b, aspect ratio ~ 6) and finally to nanocubes (Figures 2c,d, aspect ratio ~ 1). We argue that these cubes are formed by a combination of VLS and radial growth. An increase of the radial growth rate with increasing V/III ratio has been observed for other III/V semiconductors.^{13–16} However, the formation of nanocubes on top of nanowires is a surprising observation and has not been reported to our knowledge. We note that the dimensions of the cubes are determined by the growth time and diagonals ranging from 200 to 500 nm are obtained for growth times between 5 and 20 min. Structural characterization of these nanocubes reveals a pure (defect-free) zinc-blende structure as for the InSb nanowires; the details will be reported elsewhere. Figure 2e–h shows the evolution of the InSb segment when increasing the wire-to-wire distance (pitch) from 400 to 1200 nm for a constant V/III ratio of 44 and droplet diameter of 50 nm. A

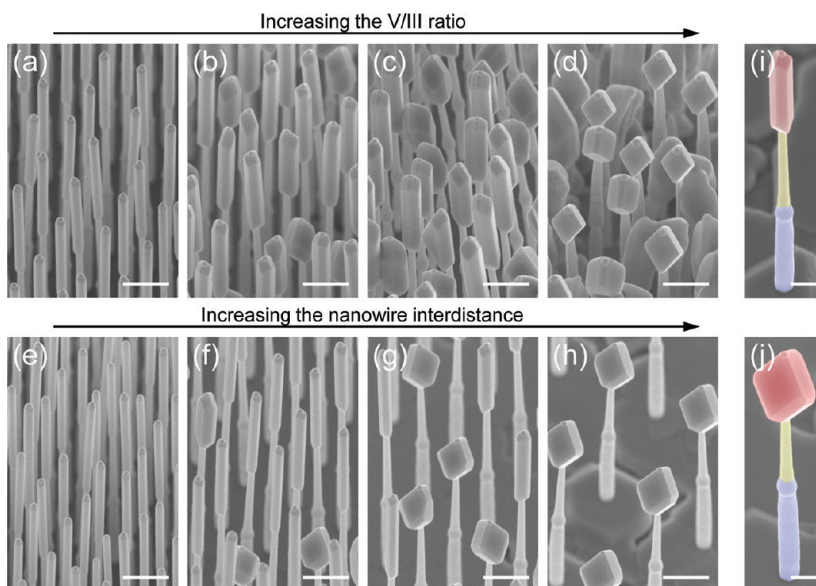


Figure 2. The 30° tilted SEM images illustrating the evolution of the InSb nanowire morphology. In all cases, the gold catalyst size is 50 nm. (a–d) Nanowire morphology as a function of the V/III ratio: (a) 44, (b) 66, (c) 88, and (d) 166 for a constant pitch of 500 nm. Scale bars correspond to 500 nm. (e–h) Nanowire morphology as a function of the pitch: (e) 400, (f) 600, (g) 800, and (h) 1200 nm for a constant V/III ratio of 44. Scale bars correspond to 500 nm. (i) Nanowire and (j) Nanocube material stacking, colors are the same as in Figure 1. Scale bars correspond to 200 nm.

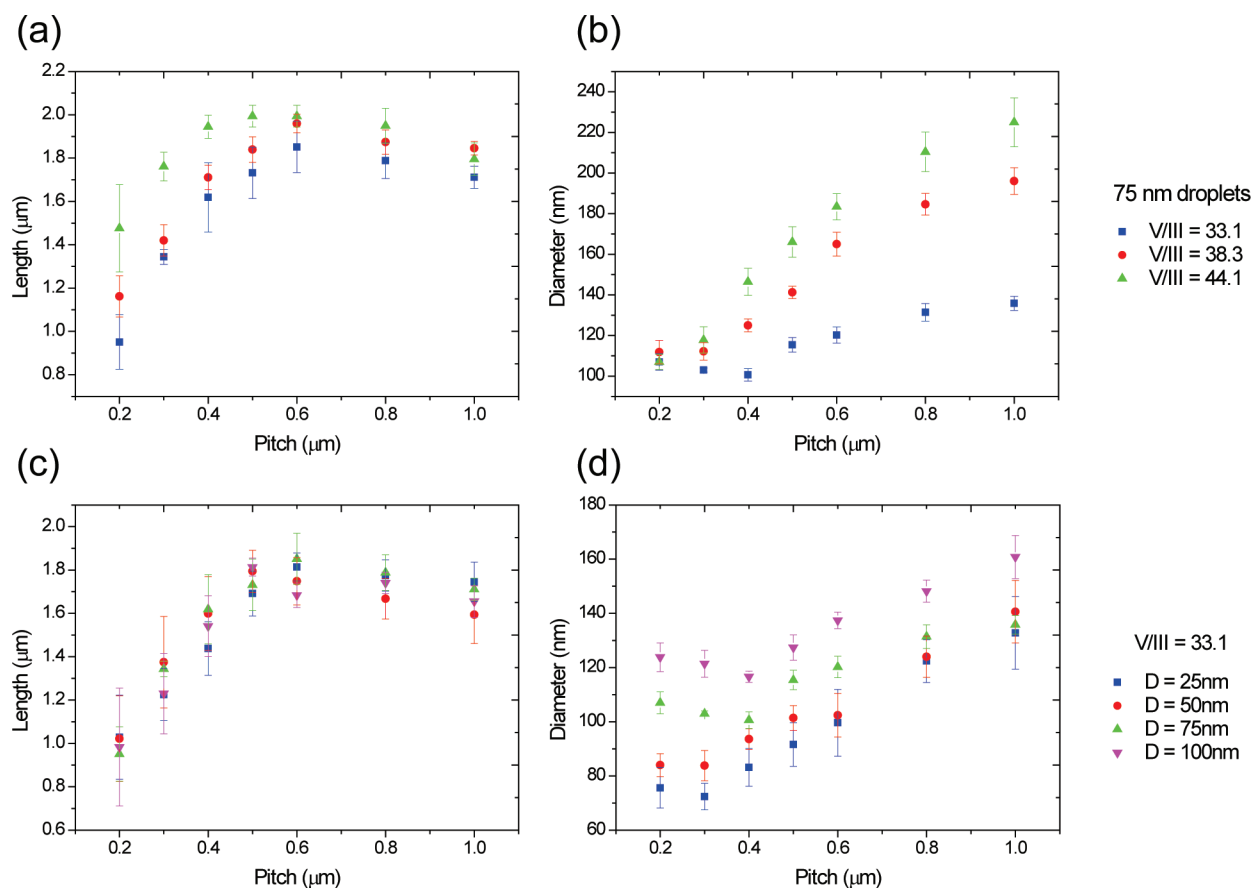


Figure 3. Statistics on the InSb nanowire arrays. At least 10 nanowires were measured for each point and the error bars represent the standard deviation. Since the InSb growth time is constant (20 min) length and vertical growth rate are equivalent. (a) Evolution of the length of the InSb segment as a function of the pitch for a droplet size of 75 nm and for different V/III ratios. (b) Evolution of the diameter of the InSb segment as a function of the pitch for a droplet size of 75 nm and for different V/III ratios. (c) Evolution of the InSb length as a function of the pitch for a V/III ratio equal to 33.1 and for different droplet sizes. (d) Evolution of the diameter in function of the pitch for a V/III ratio equal to 33.1 and for different gold diameters.

similar evolution from thin nanowires (Figure 2e) to thick nanowires (Figure 2f) and to nanocubes (Figure 2g,h) is observed. Since here the nanowire interdistance is the only variable, we conclude that the “local” V/III ratio around the nanowire depends on the nanowire density.^{17,18} This change of the V/III ratio is due to a difference in diffusion lengths of different precursors on the substrate surface (precursor diffusion is discussed in Supporting Information, Section S3). From the similarity between the structures obtained upon changing the V/III ratio and the pitch, we infer that when decreasing the density (increasing pitch), more antimony is available per wire, leading to an increase in the V/III ratio.

Quantitative data on the length and diameter of the structures are obtained from SEM pictures all taken with a 30° tilt angle along a $\langle 110 \rangle$ viewing direction from arrays aligned along the $\langle 110 \rangle$ and the $\langle \bar{1}10 \rangle$ directions of the substrate. Figure 3a shows the evolution of the InSb nanowire length (the growth time is 20 min for all samples) as a function of the pitch for a constant droplet size (75 nm) and different TMSb pressures, that is, different V/III ratios. We observe an optimum around 500 nm for which the length of the nanowires is maximum. For pitches below 500 nm, the growth rate decreases with decreasing wire-to-wire distance due to competitive growth.¹⁷ The nanowire growth rate at these small pitches increases with the Sb pressure, confirming that Sb diffusion is the rate-limiting factor for vertical growth. Thus, the

amount of antimony available per wire decreases with the pitch for the smaller interdistances. For pitches above 500 nm, the vertical growth rate decreases as well. A similar decrease has also been observed for GaP wires and was attributed to the catalytic decomposition of one of the precursors.¹⁸ Here, the latter decrease of the InSb vertical growth rate has other origins. As will be discussed below, the particle composition and the radial growth are controlled by the local V/III ratio. A higher local Sb concentration at larger pitches results in thicker and shorter nanowires.

Figure 3b shows the evolution of the nanowire diameter as a function of the pitch for a constant droplet size (75 nm) and different V/III ratios. As shown in Figure 2, increasing the V/III ratio or the pitch results in thicker nanowires. However, at the lowest V/III ratio and for pitches below 400 nm an opposite trend is observed: the diameter increases with decreasing pitch. Interestingly, the pitch at which the minimum in diameter is observed nearly coincides with the pitch at which the length is maximum (Figure 3a). This demonstrates that in order to obtain the largest aspect ratios, it is important to control the wire density. In a recent paper¹⁹ by Glas, it has been argued that the V/III ratio directly controls the droplet composition during growth. At the optimum, we find a AuIn_2 droplet composition, which is consistent with the Au/In/Sb ternary phase diagram that predicts AuIn_2 as a stable phase.²⁰ On the basis of the above, we formulate the hypothesis that if the local

antimony concentration is low (this happens at low V/III ratio and small pitches), indium is accumulated in the droplet, resulting in AuIn_x ($x > 2$) particles. Since the amount of gold is constant, indium accumulation would lead to an increase of the droplet volume and consequently to an increase of the nanowire diameter. If applied to the curve corresponding to the smallest V/III ratio in Figure 3b, this hypothesis would lead to 3 different regimes: a minimum diameter obtained for AuIn_2 droplets (at a 400 nm pitch). For smaller pitches (<400 nm), AuIn_x ($x > 2$) droplets are formed, the volume of the particle increases and consequently the nanowire diameter increases. For larger pitches (>400 nm), AuIn_xSb_y droplets are formed²¹ and both the radial growth induced by the high local V/III ratio and the increase of the particle volume lead to larger nanowire diameters. The particle composition has been investigated as a function of the pitch and is discussed in the Supporting Information, S4 section. Interestingly, if we now correlate Figure 3a,b, a sweet spot appears for which nanowires have the lowest radial and the highest axial growth rates leading to the highest aspect ratio. With further optimization of the V/III ratio and of the stem length, we obtained InSb nanowires with an improved aspect ratio of 35 (Figure 1).

Figure 3c presents the evolution of the length of the InSb wire as a function of the pitch for different droplet sizes but a constant V/III ratio (33.1). The maximum growth rate is obtained for the same pitch as in Figure 3a. The droplet diameter (ranging from 25 to 100 nm) has no significant influence on the vertical growth rate for the pitches used in this study. This is in contrast with other III/V nanowire growth reports,^{22,23} confirming that synergetic effects are not significant,¹⁸ since this would give an increased growth rate for larger particles and larger pitches. If the growth at the smallest pitches would be dominated only by the competitive mechanism, a larger vertical growth rate would be expected for the smaller particles. No diameter dependence is observed, and this could be explained by compensation of the diffusion-limited process by another mechanism. A possible candidate is the Gibbs–Thomson effect, even if its influence should be fairly small at these relatively big droplet sizes.^{24,25} Importantly, the observed vertical growth rates are significantly higher than in previous papers^{3,4,10} which is essential for increasing the InSb nanowire aspect ratio.

Figure 3d presents the evolution of the nanowire diameter as a function of the pitch for different gold particle sizes but for a constant V/III ratio (33.1). Naturally, the nanowire diameter increases with the gold particle size. A shift of the minimum diameter toward smaller pitches for smaller droplet emerges. If we assume that this minimum diameter corresponds to the AuIn_2 droplets, we can conclude that smaller droplets require a lower local V/III ratio (higher In concentration) for efficient uptake of indium, which would confirm the relevance of the Gibbs–Thomson effect. Again, at this relatively big droplet size, this effect should be relatively small but could convincingly explain the trends observed here. Energy dispersive X-ray (EDX) measurements were performed in the TEM to investigate the particle composition as a function of the wire-to-wire spacing (see Supporting Information, Section S4) in order to verify our hypothesis. We observe that the In concentration decreases slightly (from 66 to 63%) with increasing pitch, which is consistent with our hypothesis.

Finally, we assess the electronic properties of the high aspect ratio wires at low temperature (4.2 K). Ti/Au contacts for electrical transport measurements are fabricated (Figure 4a) by

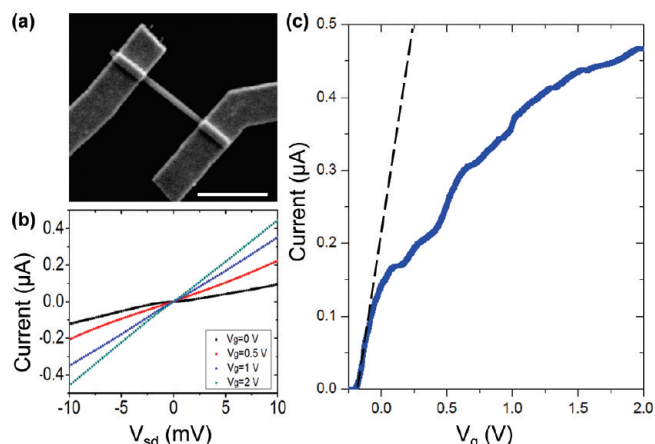


Figure 4. Electrical measurements on the InSb nanowires. (a) An SEM image of an InSb nanowire with Ti/Au source–drain contacts, lying on a 285 nm thick SiO_2 substrate. A p-doped Si layer underneath the SiO_2 acts as a global back gate. Scale bar corresponds to 1 μm . (b) Current as a function of source–drain voltage for a global gate voltage of 0, 0.5, 1, and 2 V. (c). Current through the nanowire is modulated by the voltage applied to the global back gate, source–drain bias voltage $V_{sd} = 10$ mV. The dashed line indicates the transconductance in the region near pinch-off from which the field-effect mobility is obtained. A series resistance of 15 $\text{k}\Omega$ originating from the wire-contact interface and measurement setup was subtracted. Capacitance obtained from finite elements calculations was 40 aF.

e-beam lithography. The highly doped Si substrate is used as a global gate electrode^{26,27} to control the electron density. Current–voltage characteristics reveal ohmic (linear) behavior for a wide range of gate voltages away from pinch-off (Figure 4b). To determine the electron mobility, the source–drain current I is measured at a fixed source–drain voltage $V_{sd} = 10$ mV as a function of the global gate voltage V_g as shown in Figure 4c. From the linear part of the transconductance $g_t = dI/dV_g$, the field-effect mobility $\mu = g_t l_{nw}^2 / CV_{sd}$ can be calculated, where l_{nw} is the length of the nanowire segment between the two contacts. The capacitance C between the nanowire and the back gate is estimated from a finite elements model that includes charge screening from source and drain contacts.^{28,29} Mobilities are determined for six devices and values ranging from 2.0×10^4 to 3.5×10^4 $\text{cm}^2 \text{V}^{-1} \text{s}^{-1}$ are obtained. For an electron density of $1 \times 10^{17} \text{cm}^{-3}$, a mean free path of 260 nm is calculated. The mean free path exceeds the nanowire diameter of ~ 100 nm suggesting a quasi-ballistic transport regime with multiple specular reflections. These mobilities are the highest reported so far for InSb nanowires^{6,30} but much lower than that of bulk material. Possible mechanisms for electron scattering, reducing the mobility, include surface roughness and impurity induced disorder inside the nanowires. For few devices, a sulfur passivation of the wire was performed, prior to covering them with SiO_2 ³¹ but no influence on mobilities is observed.

In conclusion, we report optimized growth conditions that lead to InSb nanowires with an aspect ratio up to 35. We demonstrate that the V/III ratio and the nanowire interdistance have the same influence on the local environment and can change the InSb shape from thin nanowires to nanocubes. InSb lengths and diameters are systematically measured leading to complete statistics on the growth conditions. A sweet spot in growth parameters is revealed for which thinner and longer wires can be grown. We suggest that the growth conditions

change the catalyst composition and that an optimum is reached for AuIn₂ droplets. More generally, we propose a method for optimizing the InSb nanowire shape for electronic devices and show electrical measurements proving the high quality of InSb nanowires. Finally, we report the first nanocubes grown on top of nanowires, opening new possibilities of 3D integration.

■ ASSOCIATED CONTENT

■ Supporting Information

Additional information and figures. This material is available free of charge via the Internet at <http://pubs.acs.org>.

■ AUTHOR INFORMATION

Corresponding Author

*E-mail: s.r.plissard@tue.nl.

Notes

The authors declare no competing financial interest.

■ REFERENCES

- (1) Nadj-Perge, S.; Frolov, S. M.; Bakkers, E. P. A. M.; Kouwenhoven, L. P. *Nature* **2010**, *468*, 1084–1087.
- (2) Caroff, P.; Messing, M. E.; Borg, M.; Dick, K. A.; Deppert, K.; Wernersson, L. E. *Nanotechnology* **2009**, *20*, 495606.
- (3) Lugani, L.; Ercolani, D.; Rossi, F.; Salviati, G.; Beltram, F.; Sorba, L. *Cryst. Growth Design* **2010**, *10*, 4038–4042.
- (4) Vogel, A. T.; de Boor, J.; Wittemann, J. V.; Mensah, S. L.; Werner, P.; Schmidt, V. *Cryst. Growth Design* **2011**, *11*, 1896–1900.
- (5) Nilsson, H. A.; Caroff, P.; Thelander, C.; Lind, E.; Karlström, O.; Wernersson, L. E. *Appl. Phys. Lett.* **2010**, *96*, 153505.
- (6) Wang, Y.; Chi, J.; Banerjee, K.; Grützmacher, D.; Schäfers, T.; Lu, J. G. *J. Mater. Chem.* **2011**, *21*, 2459.
- (7) Khan, M. I.; Penchev, M.; Jing, X.; Wang, X.; Bozhilov, K. N.; Ozkan, M.; Ozkan, C. S. *J. Nanoelectron. Optoelectron.* **2008**, *3*, 199–202.
- (8) Paul, R. K.; Penchev, M.; Zhong, J.; Ozkan, M.; Ghazinejad, M.; Jing, X.; Yengel, E.; Ozkan, C. S. *Mater. Chem. Phys.* **2010**, *121*, 397–401.
- (9) Nilsson, H. A.; Caroff, P.; Thelander, C.; Larsson, M.; Wagner, J. B.; Wernersson, L. E.; Samuelson, L.; Xu, H. Q. *Nano Lett.* **2009**, *9*, 3151–3156.
- (10) Caroff, P.; Wagner, J. B.; Dick, K. A.; Nilsson, H. A.; Jeppsson, M.; Deppert, K.; Samuelson, L.; Wallenberg, R.; Wernersson, L. E. *Small* **2008**, *4*, 878–882.
- (11) Lutchyn, F. M.; Sau, J. D.; Das Sarma, S. *Phys. Rev. Lett.* **2010**, *105*, 077001.
- (12) Oreg, Y.; Rafael, G.; von Oppen, F. *Phys. Rev. Lett.* **2010**, *105*, 17702.
- (13) Persson, A. I.; Ohlsson, B. J.; Jeppesen, S.; Samuelson, L. *J. Cryst. Growth* **2004**, *272*, 167–174.
- (14) Dayeh, S. A.; Yu, E. T.; Wang, D. *Nano Lett.* **2007**, *7*, 2486–2490.
- (15) Borgström, M. T.; Wallentin, J.; Trägårdh, J.; Ramvall, P.; Ek, M.; Wallenberg, L. R.; Samuelson, L.; Deppert, K. *Nano Res.* **2010**, *3*, 264–270.
- (16) Plissard, S.; Dick, K. A.; Larrieu, G.; Godey, S.; Addad, A.; Wallart, X.; Caroff, P. *Nanotechnology* **2010**, *21*, 385602.
- (17) Jensen, L. E.; Björk, M. T.; Jeppesen, S.; Persson, A. I.; Ohlsson, B. J.; Samuelson, L. *Nano Lett.* **2004**, *4*, 1961–1964.
- (18) Borgström, M. T.; Immink, G.; Ketelaars, B.; Algra, R.; Bakkers, E. P. A. M. *Nat. Nanotechnol.* **2007**, *2*, 541–544.
- (19) Glas, F. *J. Appl. Phys.* **2010**, *108*, 073506.
- (20) Liu, H. S.; Liu, C. L.; Wang, C.; Jin, Z. P.; Ishida, K. *J. Electron. Mater.* **2003**, *32*, 81–88.
- (21) Yang, X.; Wang, G.; Slattery, P.; Zhang, J. Z.; Li, Y. *Cryst. Growth Design* **2010**, *10*, 2479–2482.
- (22) Kashchiev, D. *Cryst. Growth Design* **2006**, *6*, 1154–1156.
- (23) Fröberg, L. E.; Seifert, W.; Johansson, J. *Phys. Rev. B* **2007**, *76*, 153401.
- (24) Dayeh, S. A.; Picraux, S. T. *Nano Lett.* **2010**, *10*, 4032–4039.
- (25) Johansson, J.; Dick, K. A.; Caroff, P.; Messing, M. E.; Bolinsson, J.; Deppert, K.; Samuelson, L. *J. Phys. Chem. C* **2010**, *114*, 3837–3842.
- (26) Scheffler, M.; Nadj-Perge, S.; Kouwenhoven, L. P.; Borgström, M. T.; Bakkers, E. P. A. M. *Physica E* **2008**, *40*, 1202.
- (27) van Tilburg, J. W. W.; Algra, R. N.; Verheijen, M.; Immink, G.; Bakkers, E. P. A. M.; Kouwenhoven, L. P. *Semicond. Sci. Technol.* **2010**, *25*, 024011.
- (28) Zwaneburg, F. A.; van Loon, A. A.; Steele, G. A.; van Rijmenam, C. E. W. N.; Balder, T.; Fang, Y.; Lieber, C. M.; Kouwenhoven, L. P. *J. Appl. Phys.* **2009**, *105*, 124314.
- (29) Wunnicke, O. *Appl. Phys. Lett.* **2006**, *89*, 083102.
- (30) Philipose, U.; Sapkota, G.; Salfi, J.; Ruda, H. E. *Semicond. Sci. Technol.* **2010**, *25*, 075004.
- (31) Suyatin, D. B.; Thelander, C.; Björk, M. T.; Maximov, I.; Samuelson, L. *Nanotechnology* **2007**, *18*, 105307.